Journal of Chromatography A, 1218 (2011) 1592–1602

Contents lists available at ScienceDirect

Journal of Chromatography A

journal homepage: www.elsevier.com/locate/chroma

Kinetic investigation of the relationship between the efficiency of columns and their diameter

Fabrice Gritti, Georges Guiochon*

Department of Chemistry, University of Tennessee, Knoxville, TN 37996-1600, USA

ARTICLE INFO

Article history:
Available online 14 December 2010

Keywords:
Shell particles
Column efficiency
Narrow-bore column
Eddy diffusion
Kinetex
Poroshell120
Halo
Naphthalene

ABSTRACT

Many brands of packing materials made of fine particles are now available in both conventional (4.6 mm i.d.) and narrow-bore (2.1 mm i.d.) columns. It is a general observation that the efficiency of the former tends to be markedly higher than that of the latter. This report provides a detailed illustration of the characteristics of this enigma. The corrected reduced plate heights of three brands of columns packed with shell particles in 4.6 and 2.1 mm I.D. columns were measured. The brands were the 1.7 and 2.6 μm Kinetex-C_{18} (Phenomenex, Torrance, CA, USA), the 2.7 μm Poroshell120-C_{18} (Agilent Technologies, New Castle, DE, USA), and the 2.7 μm Halo-C_{18} (Advanced Material Technologies, Wilmington, DE, USA). The extra-column contributions were minimized by optimizing the configuration of the instrument (injection volume < 1.0 μL, 115 μm needle seat capillary, 80 μm connecting tubes, no heat exchanger, 0.8 μL detection cell). The correct peak variances were derived from the numerical integration of the first and second order moments of the experimental band profiles. These experimental results confirm that the kinetic performance of narrow-bore columns is inferior to that of conventional columns for all three brands of shell particles. We demonstrate that this difference is accounted for by a contribution to the column HETP of the long-range eddy diffusion term that is larger in the 2.1 than in the 4.6 mm I.D. columns. While the associated relative velocity biases are of comparable magnitude in both types of columns, the characteristic radial diffusion lengths are of the order of 100 and 40 μm in the wall regions of narrow-bore and conventional columns, respectively.

1. Introduction

When high performance liquid chromatography (HPLC) began, in the mid 1960s, the first columns were packed with 50 μm particles, using dry-packing methods. They provided efficiencies of no more than 5000 plates/m. Currently, columns are packed with either sub-2 μm fully porous particles [1,2] or sub-3 μm superficially porous particles [3–8], using slurry packing methods. They are operated with high-pressure solvent delivery systems (at >1000 bar). These columns can provide close to 300,000 plates/m, at speeds two orders of magnitude larger. These gains are largely due to the 20-fold decrease in the average particle size; the actual contribution of better packing methods has contributed by a factor of nearly 3. This progress was made possible by considerable improvements in instrument design.

It is important to underline that this high efficiency is only achieved for either highly retained compounds on large I.D. columns (4.6 mm) or after correction of the observed efficiency for the extra-column contributions due to the instrument. In other words, analysts can record separations reflecting column efficiencies of more than 300,000 plates/m only if the extra-column contribution to band broadening is negligible compared to the band width of the eluted analytes. Such a high level of column efficiency has rarely been reported for unretained compounds on any 4.6 mm I.D. column or for weakly retained compounds on narrow-bore columns, even with the most recent very high-pressure instruments, which have been designed to provide smaller extra-column peak variances than the conventional 400 bar instruments [9,10]. The significant contributions of these modern instruments to band broadening are consistent with the use of narrow-bore columns only for analyses carried out under gradient elution conditions. These contributions remain significant with poorly retained samples and when narrow-bore columns are used under isocratic conditions.

When columns packed with sub-2 μm fully porous or sub-3 μm superficially porous particles are used at reduced velocities in the range $10 < \nu < 20$, under quasi-adiabatic conditions, the minimum corrected reduced plate height is of the order of 1.4 for 4.6 mm I.D. columns packed with 2.6–2.7 μm shell particles [5,6] and around 2.0 for 2.1 mm I.D. columns packed with 1.7 μm fully porous par-

* Corresponding author at: Department of Chemistry, University of Tennessee, 414 Buehler Hall, Knoxville, TN 37996-1600, USA. Tel: +1 865 974 0733; fax: +1 865 974 2667.
E-mail address: guiochon@utk.edu (G. Guiochon).

0021-9673/$ – see front matter © 2010 Elsevier B.V. All rights reserved.
doi:10.1016/j.chroma.2010.12.023

ticles [2]. The contributions[1] of the longitudinal diffusion term (B/ν) for retained compounds are smaller than 0.3 and 0.4 with shell and fully porous particles, respectively, [8,11]. In this range of reduced velocities, the longitudinal diffusion term decreases and the solid–liquid mass transfer resistance term increases with increasing reduced velocity. These two effects cancel out and their sum remains nearly constant at about 0.7 [8]. Thus, 50 and 65% of the reduced plate heights of the columns packed with the shell and the fully particles, respectively, is accounted for by the eddy diffusion term (A), which is the major contribution to the total reduced HETP.

As shown by Giddings, the A term of packed beds is related to three different and independent sources of velocity unevenness in the stream flowing through the interstitial column volume: (1) the trans-channel (between adjacent particles); (2) the short-range inter-channel (over a distance of a few particle diameters); and (3) the trans-column (over the column inner radius) velocity biases [12]. The contributions of the first two of these velocity inequalities seem to be independent of the size distributions of the particles when they are arranged in a randomly packed bed [13], so they should be similar whether the relative standard deviation of this distribution is $\simeq$ 20% as with fully porous particles or $\simeq$ 5% as with shell particles. For linear velocities between 10 and 20, the sum of the reduced HETP terms related to trans-channel and inter-channel velocity biases is nearly constant around 0.5 [12,14,8]. In conclusion, the main difference between the reduced plate heights of 2.1 mm I.D. columns packed with fully porous particles ($h = 2.0$) and 4.6 mm I.D. columns packed with shell particles ($h = 1.4$) can only originate in the contribution of the trans-column velocity biases to the overall reduced plate height, which are roughly 0.8 and 0.2, respectively). Experimental data aiming at isolating the eddy diffusion term in packed beds [11,15] show that the overall reduced eddy diffusion HETP terms of 4.6 mm I.D. columns packed with shell and fully porous particles of the same size are 0.8 and 1.4, respectively, at the optimum velocity. The difference in the contributions of eddy diffusion in the two types of packing material is thus directly related to the extent of the radial heterogeneity of the packed bed at the scale of the column radius.

In conclusion, the 4.6 mm I.D. beds packed with 2.6–2.7 μm superficially particles are more homogeneous than those of the 2.1 mm I.D. narrow-bore beds packed with 1.7 μm fully porous particles. The external roughness of the core–shell particles might explain the origin of this advantageous property because the shear stress that takes place during the slurry packing process is stronger between rugged particles than between smooth ones. Therefore, particles move less by respect to each other and the amount of strain occurring through the bed is smaller. Thus, the distribution of the external porosity throughout the bed of rugged particles is more homogeneous from the center (low packing stress) to the wall of the column (high packing stress) than through beds of smooth particles [16]. The radial packing homogeneity in narrow-bore columns has never been investigated with shell particles. In a recent review on the art and science of forming packed analytical HPLC columns [17], the author did not discuss the formation of packed beds with different packing materials but only with columns of various inner diameters.

In this work, we compare the kinetic performances of three brands of core–shell particles (2.7 μm Halo from Advanced Material Technology, 1.7 and 2.6 μm Kinetex from Phenomenex, and 2.7 μm Poroshell120 from Agilent Technologies) when packed in 4.6 and 2.1 mm I.D. columns. An exact correction for the extra-column volume contributions was performed by meticulously calculating by numerical integration the first and second central moments of each experimental band profile eluted through the column and through a zero volume connector and subtracting the corresponding moments. The trans-column eddy diffusion term is then determined. It provides useful conclusions on the effect of the column inner diameter on the radial packing homogeneity of beds of sub-3 μm shell particles.

2. Theory

2.1. Theoretical HETP of columns packed with shell particles

The general plate height equation, $h = f(\nu)$, for columns packed with totally or superficially porous particles was recently derived [11]. It includes the classical longitudinal diffusion term (B/ν), derived from the general effective medium theory of Landauer [18] extended to molecular diffusion [19] and applied to the problem of axial diffusion in heterogeneous packed HPLC beds [20], the total eddy diffusion term, $A(\nu)$, accounting for trans-channel, short-range inter-channel, and trans-column unevenness in the flow velocity in the packed bed volume, the trans-particle mass transfer resistance term, $C_p\nu$, the external film mass transfer resistance term, $C_f\nu$, and the additional reduced HETP term, h_{Heat}, accounting for the efficiency loss caused by the formation of radial temperature gradients across the column diameter at high flow rates and pressure drops [21,22]. This general equation clearly elucidates the relationships between the different components of the mass transfer resistance and the relevant physico-chemical parameters characterizing the column bed and the separation involved [8]. It is written as:

$$h = \frac{B}{\nu} + A(\nu) + C_p\nu + C_f(\nu)\nu + h_{Heat} \tag{1}$$

The detailed form of this equation in which the different terms are explicited but the frictional heating effects are neglected is written:

$$h = \frac{2}{\epsilon_e}\frac{\left[a + \sqrt{a^2 + 1/2\Omega(1-\rho^3)}\right]}{\nu}$$

Longitudinal molecular diffusion (2)

$$+\frac{0.0045\nu}{1+0.005\nu}$$ Trans-channel eddy diffusion (3)

$$+\frac{0.15\nu}{1+0.3\nu}$$ Short-range inter-channel eddy diffusion (4)

$$+\frac{1}{1/\lambda_3 + 1/\omega_3\nu}$$ Trans-column eddy diffusion (5)

$$+\frac{1}{30}\frac{\epsilon_e}{1-\epsilon_e}\left[\frac{k_1}{1+k_1}\right]^2\frac{1+2\rho+3\rho^2-\rho^3-5\rho^4}{\left(1+\rho+\rho^2\right)^2}\frac{1}{\Omega}\nu$$

Trans-particle mass transfer (6)

$$+\frac{1}{3}\frac{\epsilon_e}{1-\epsilon_e}\left[\frac{k_1}{1+k_1}\right]^2\frac{1}{Sh}\nu$$ External film mass transfer (7)

In this equation, ϵ_e is the external porosity of the packed bed, ρ the ratio of the solid core diameter to that of the core–shell particle ($\rho = 0$ for fully porous particles), λ_3 and ω_3 are positive parameters related to the contribution of trans-column velocity biases to the column HETP [12], $\nu = ud_p/D_m$ is the reduced interstitial linear velocity (u is the interstitial linear velocity, d_p the average particle diameter, and D_m the sample diffusion coefficient in the bulk), Ω

[1] NB. All the contributions to the reduced HETP given in this paper are dimensionless.

is the ratio of the effective sample diffusivity in the porous shell to the bulk sample diffusion coefficient, $Sh = (1.09/\epsilon_e^{2/3})\nu^{1/3}$ is the Sherwood number, and k_1 is the zone retention factor [23]:

$$k_1 = \frac{1-\epsilon_e}{\epsilon_e}\left[\epsilon_p + (1-\epsilon_p)K\right](1-\rho^3) \quad (8)$$

where ϵ_p is the porosity of the shell and K is the distribution coefficient of the sample between the porous layer in the shell and the liquid phase. In the first term of the right-hand-side of Eq. (2) (longitudinal molecular diffusion term), the parameter a is written [20]:

$$a = \frac{1}{4}\left[3\epsilon_e - 1 + \Omega(2-3\epsilon_e)\right] \quad (9)$$

Finally, the numerical parameters accounting for the eddy diffusion terms related to the trans-channel (0.0045 and 0.005) and short-range inter-channel (0.15 and 0.30) velocity biases were taken from the reference [14]. They are based on a statistical analysis of randomly packed beds (Voronoi volume) and on the Gidding's equation for bulk packings. These values were taken for an external porosity $\epsilon_e = 0.40$ (actual external porosity of columns packed with shell particles) and for the so-called S-packing. The S-packing was generated from a box initially divided into n equal cubic cells with each particle center placed in a random position in a cell. Note that the short-range inter-channel parameters were assumed to be the same for all the columns tested, because the external porosities of their beds are about the same, at $0.40 < \epsilon_e < 0.42$. The calculation results of Tallarek et al. [14] show that the relative variations of λ_2 and ω_2 are very small (< 5 and 15%, respectively) for the S-packing configuration when the external porosity is increased from 0.40 to 0.42.

2.2. Heat friction power

The power heat friction, P_f, liberated per unit length of the column is given by [24]:

$$P_f = F_v \frac{\Delta P}{L} \quad (10)$$

where F_v is the flow rate, ΔP is the pressure drop along the column (the pressure drop caused by the instrument should be subtracted to the total pressure drop), and L is the column length.

Note that heat friction effects become significant in large I.D. columns (4.6 mm I.D.) because these columns can be operated at high flow rates. Yet, one of the great advantages of the columns packed with shell particles over those packed with fully porous particles is that the heat conductivity of their bed is higher, which reduces the amplitude of the radial temperature gradients and minimizes the loss of efficiency due to the radial thermal heterogeneity [21,22]. This will be discussed later in the results and discussion section.

2.3. Peak variances

The increase in band width caused by the migration of a sample zone along a chromatographic column can be derived by summing up the increment of zone variance between the column entrance and its exit. Under isocratic conditions, this contribution, $\sigma^2_{v,col.}$, to the total peak variance measured at the detector exit is written in volume unit squared [10] as:

$$\sigma^2_{v,col.} = \frac{V_0^2}{N}(1+k)^2 \quad (11)$$

where V_0 is the column hold-up volume, N its efficiency, and k the retention factor of the sample.

Band broadening also occurs in the different parts of the HPLC system, including its injection and detection components and the connecting tubes. The complex peak variance, $\sigma^2_{v,ex}$, results from axial dispersion along the channel followed by the sample plug. This channel is made of a series of connecting tubes with their nooks and crannies. Their behavior is difficult to model accurately. An empirical model based on the coupling between axial dispersion in the stream flowing along a straight tube and radial diffusion through a side cavity was proposed to account for dispersion in these channels [25]. Yet, the effect of stagnant zones of eluent located at the connections between different parts of the system seems impossible to model accurately enough. These dead volumes are particularly harmful in gradient elution because they contribute significantly to increase the time necessary to re-equilibrate the column between two consecutive injections. Consequently, it is required that the extra-column peak variance be determined experimentally for a given sample, a given eluent, and a known temperature.

The observed peak variance of the band profile recorded, $\sigma^2_{v,obs}$, is the sum of the column and the system contributions. Therefore,

$$\sigma^2_{v,obs} = \sigma^2_{v,ex} + \sigma^2_{v,col.} \quad (12)$$

In this work, we measured $\sigma^2_{v,obs}$ (in the presence of the chromatographic column) and $\sigma^2_{v,ex}$ (in the presence of a zero dead volume union connector which replaces the column).

3. Experimental

3.1. Chemicals

The mobile phase was a mixture of water and acetonitrile (30/70, v/v). These two solvents were HPLC grade from Fisher Scientific (Fair Lawn, NJ, USA). The mobile phase was filtered before use on a surfactant-free cellulose acetate filter membrane, 0.2 μm pore size (Suwannee, GA, USA). The sample was naphthalene and the hold-up volume marker uracil, both purchased from Aldrich (Milwaukee, WI, USA).

3.2. Columns

Nine different columns were used in this work. Three 2.7 μm Poroshell120-C_{18} columns (150 × 4.6, 100 × 2.1, and 50 × 2.1 mm) were generously offered by the column manufacturer (Agilent Technologies, New Castle, DE, USA). Two 1.7 μm Kinetex-C_{18} columns (100 × 4.6, and 150 × 2.1 mm) and two 2.6 μm Kinetex-C_{18} columns (150 × 4.6, and 150 × 2.1 mm) were provided by the column manufacturer (Phenomenex, Torrance, CA, USA). Finally the two 2.7 μm Halo-C_{18} columns (150 × 4.6, and 150 × 2.1 mm) were purchased from Advanced Material Technology (Wilmington, DE, USA).

The hold-up volumes of these nine columns were estimated from the corrected elution volumes of uracil in acetonitrile/water (70/30, v/v) extrapolated to a flow rate equal to zero. Note that the hold-up volumes measured by pycnometry are typically 10 % larger than those measured by the elution time of the unretained tracer, due to the slight size exclusion of the tracer from the internal volume of the porous shell. The total porosities, other physicochemical properties (specific surface area, average pore size, mean particle diameter, particle size distribution ratio $d_{90\%}/d_{10\%}$), the batch numbers of the packing materials, and the column serial numbers are given in Table 1. The estimated retention factors of naphthalene are listed in Table 2.

3.3. HPLC system

All the data were acquired with the Agilent 1290 Infinity HPLC system (Agilent Technology, Waldbronn, Germany) liquid chromatograph. This instrument includes a binary pump with solvent

Table 1
Physico-chemical properties of the Halo and Kinetex columns given by the manufacturer and measured in our lab. [a]

	Halo 90 Å		Kinetex 100 Å				Poroshell 120 Å		
SEM mean particle size [μm]	2.7	2.7	1.7	1.7	2.6	2.6	2.7	2.7	2.7
$\rho = R_i/R_e$	0.63	0.63	0.71	0.71	0.73	0.73	0.63	0.63	0.63
Pore diameter [Å]	90	90	100	100	100	100	120	120	120
Surface area [m^2/g]	150	150	200	200	200	200	120	120	120
Particle size distribution ($d_{90\%-10\%}$)	1.13	1.13	1.12	1.12	1.12	1.12	1.13	1.13	1.13
Batch / Serial number	AH092259 / USNR001558	AH092221 / USFH00129	5574-28 / 507292-26	5574-31 / 17677	5569-110 / 51841-8	5569-115 / 520673-6	B10085 / USGGE01078	B10085 / USGGC01052	B10120 / USCFR01202
Dimension (mm × mm)	2.1 × 150	4.6 × 150	2.1 × 150	4.6 × 100	2.1 × 150	4.6 × 150	2.1 × 50	2.1 × 100	4.6 × 150
Total porosity [a]	0.466	0.466	0.480	0.467	0.473	0.474	0.505	0.505	0.487

[a] Estimated from the corrected elution time of uracil in CH_3CN/H_2O (70/30, v/v).

Table 2
Maximum column pressure drops, flow rates, and power friction liberated in the nine columns. [a]

	Halo 90 Å		Kinetex 100 Å				Poroshell 120 Å		
SEM mean particle size [μm]	2.7	2.7	1.7	1.7	2.6	2.6	2.7	2.7	2.7
Dimension (mm × mm)	2.1 × 150	4.6 × 150	2.1 × 150	4.6 × 100	2.1 × 150	4.6 × 150	2.1 × 50	2.1 × 100	4.6 × 150
Maximum flow rate [mL/min]	0.667	3.200	0.542	3.200	0.667	3.200	0.667	0.667	3.200
Maximum column pressure drop [bar]	425	440	974	570	474	578	222	385	580
Maximum power heat friction [W/m]	3.1	15.6	5.8	30.4	3.5	20.6	4.9	4.3	20.6
Retention factor naphthalene k [a]	2.04	2.08	1.50	1.63	1.63	1.61	2.04	2.04	2.03
k_1	1.91	1.94	1.28	1.33	1.29	1.28	2.13	2.13	2.02
$C_{exp}(\nu = 10 \rightarrow 20)$	0.070	0.045	0.123	0.042	0.065	0.036	0.089	0.091	0.056
C_p	0.006	0.006	0.003	0.003	0.003	0.003	0.006	0.006	0.006
$C_f(\nu = 10)$	0.022	0.022	0.016	0.017	0.016	0.016	0.024	0.024	0.023
Ω	1.03	1.03	0.97	1.02	1.09	1.20	0.86	0.87	0.74
ω_3	0.13	0.06	1.52	0.23	0.08	0.03	0.35	0.52	0.03
λ_3	1.35	1.55	1.28	1.50	0.98	1.10	0.80	1.27	1.45
d_{tc}/d_p	26	17	87	34	20	12	42	51	13

[a] Hold-up time estimated from the corrected elution time of uracil in CH_3CN/H_2O (70/30, v/v).

selection valves, an auto-sampler with a 20 μL sample loop, a small volume needle seat capillary (1.2 μL), a column thermostat, and a Chemstation data software. The standard configuration of this system was optimized in order to minimize the contribution of the extra-column band broadening to the variance measured for the peaks eluted from the chromatographic column [9]. This system configuration includes a 100 mm × 115 μm needle seat capillary, a 250 mm × 80 μm inlet capillary tube, a 250 mm × 80 μm outlet capillary tube, and a UV-detector cell (0.8 μL). Since all the experiments were made at room temperature, the 1.6 μL heat exchanger was deliberately by-passed in order to further minimize the extra-column band broadening contribution. The signal sampling rate was set at 160 Hz for the measurement of all extra-column band profiles and at 80 and 40 Hz for the measurement of the band profiles eluted from the 2.1 and 4.6 mm I.D. columns, respectively. The columns were all let free in still-air condition. Each recorded profile includes at least 60 data points or 15 data points per peak standard deviation, σ. More than 15 data points per peak standard deviation does not result in any change of the second central moments measured by the full integration method (see later).

The high level of the reproducibility achieved by the 1290 Infinity HPLC system in the delivery of a 0.20 μL sample volume with a 20 μL sample loop, 5% in relative standard deviation for 1% of the loop volume, is truly remarkable.

The flow rate accuracy was checked at ambient temperature by directly collecting the mobile phase in the absence of the column at 295 K and at flow rates of 0.1, 1.0, and 5.0 mL/min during 50, 25, and 10 min, respectively. The relative errors were all less than 0.3%, so we estimate the long-term accuracy of the flow-rate at 3 μL/min or better at flow rates around 1 mL/min. The laboratory temperature was controlled by an air conditioning system set at 22 °C. The daily variation of the ambient temperature never exceeded ±1 °C.

3.4. Sample preparation and injection volumes

One 2 mL vial containing naphthalene and traces of uracil was prepared by dissolving 4.3 mg of naphthalene in 10 mL of pure acetonitrile. The vial was filled by pipetting 1260 μL of this naphthalene acetonitrile solution and adding 540 μL of pure water. Traces of uracil were added with a thin spatula.

The sample vial concentration was successively diluted by a factor 1/2 until the maximum absorption signal of the peak apex recorded was smaller than 1500 mAU at a flow rate of 0.1 mL/min. After three successive dilutions, the final injected concentration of naphthalene was 375 μg/L.

Volumes of 0.21 and 1.0 μL of this sample were injected into the 2.1 mm and 4.6 mm I.D. columns, respectively, in order to keep constant the sample loading per unit of column cross-section area.

3.5. Measurement of the HETP data

The peak responses of naphthalene were recorded at a wavelength of 254 nm. The detector bandwidth was fixed at 4 nm.

The sequence of flow rates was 0.021, 0.042, 0.063, 0.083, 0.125, 0.167, 0.208, 0.250, 0.292, 0.333, 0.375, 0.417, 0.479, 0.542, 0.604, and 0.667 mL/min with the 2.1 mm I.D. columns and 0.10, 0.20, 0.30, 0.40, 0.60, 0.80, 1.00, 1.20, 1.40, 1.60, 1.80, 2.00, 2.30, 2.60, 2.90, and 3.20 mL/min with the 4.6 mm I.D. columns. The sequence of linear velocities was kept the same with all columns. The reduced velocity was derived from the value of the diffusion coefficient of

naphthalene in a mixture of water and acetonitrile (30/70, v/v) according to the Wilke and Chang correlation [26] (D_m=1.11 × 10^{-5}cm^2/s). Given the possible error made on the diffusion coefficient (±10%), the external porosity was assumed to be the same at ϵ_e=0.40 for all the columns tested. The external porosity of columns packed with C_{18}-bonded shell particles, measured by inverse size-exclusion chromatography (ISEC) varies consistently between 0.39 and 0.41 [8].

For each of these 32 flow rates and for each sample, the extra-column contributions to the retention volume and to the band broadening of the probe, naphthalene, were measured by replacing the chromatographic column with a zero-volume (ZDV) union connector.

The experimental HETP data measured for the columns were corrected for the contribution of the 1290 Infinity HPLC system to band broadening. The extra-column and the total band variances were measured by numerical integration of the elution profiles to calculate their first and second order moments. Prior to any measurement, each profile recorded was corrected for baseline drift, then split around its apex, into a left and a right. Then, the first and second central moments of the two halfs of the concentration profiles were calculated in an Excel spread-sheet and given by:

$$\mu_1 = \frac{\sum_{i=1}^{i=N-1} (C_i + C_{i+1})(t_i + t_{i+1})}{2\sum_{i=1}^{i=N-1} C_i + C_{i+1}} \quad (13)$$

$$\mu_2^{'} = \frac{\sum_{i=1}^{i=N-1} (C_i + C_{i+1})\left(\frac{t_i+t_{i+1}}{2} - \mu_1\right)^2}{\sum_{i=1}^{i=N-1} C_i + C_{i+1}} \quad (14)$$

where N is the number of data points (t_i, C_i) after the left and right cut-off.

The corrected reduced HETP, h, is then given by:

$$h = \frac{L}{d_p}\frac{\mu_2^{'} - \mu_{2,ex}^{'}}{\left(\mu_1 - \mu_{1,ex}\right)^2} \quad (15)$$

where L is the column length, d_p the mean particle size, and $\mu_{1,ex}$ and $\mu_{2,ex}^{'}$ are the first and the second central moments of the corresponding extra-column band profiles. As will be demonstrated in a forthcoming paper, this method is correct and should replace the incorrect, poorly approximate, inaccurate method consisting in measuring the correction from the peak widths at mid-height [27].

The precision of the h data is given by

$$\left|\frac{\Delta h}{h}\right| = \left|\frac{\Delta\mu_2^{'}}{\mu_2^{'}}\right|\left(\frac{\mu_2^{'} + \mu_{2,ex}^{'}}{\mu_2^{'} - \mu_{2,ex}^{'}}\right) + 2\left|\frac{\Delta\mu_1}{\mu_1}\right|\left(\frac{\mu_1 + \mu_{1,ex}}{\mu_1 - \mu_{1,ex}}\right) \quad (16)$$

The second and first moments of the tracer peak, $\mu_2^{'}$ and μ_1, were measured for three successive injections, first with the chromatographic column, then with a zero-volume connector fitted to the instrument. The relative errors made on these moments were always less than 3 and 0.5%, for the second and the first moments, respectively. Note that it is the excellent level of repeatability of the injection system of the 1290 Infinity system that permits this excellent precision. Actually, the precision of the integration method depends essentially on the left and right cut-off abscissa. The 3% precision was obtained when these abscissa were identical for all three injections, again possible because the flow rate delivered by the pump of the instrument is really constant. However, when the flow rate is changed, so are the cut-off abscissa and the precision of the peak variance plotted as a function of the flow rate may seem lesser. Yet, this integration approach (use of Eq. 13) provides the most accurate HETP data that the analyst can get [27] and is much more accurate than other approximate approaches such as the half-height peak width and/or the peak fitting methods.

Accordingly, if the extra-column contributions were to be negligible, the largest random error would be of the order of 4%. This is typically the case with large volume columns. This contribution affects particularly narrow, short columns. For instance, if $\mu_2^{'}$ were to be only twice $\mu_{2,ex}^{'}$ on a new column and μ_1 were about ten times $\mu_{1,ex}$, the maximum random error becomes close to 10%.

4. Results and discussion

In the first part of this work, we determine the maximum heat power generated by viscous friction in each column tested. For this purpose, narrow-bore and 4.6 mm I.D. columns were run at maximum flow rates of 0.667 and 3.2 mL/min, respectively. In a second part, the derivation of the characteristic parameters of the general HETP Eq. (2) is discussed. This equation is fitted to the experimental HETP data, providing estimates of the best values of the coefficients Ω (ratio of the sample diffusivity in the shell to the molecular diffusion coefficient in the bulk mobile phase), ω_3 (eddy diffusion parameter related to the trans-column velocity biases controlled by a diffusion mechanism), and λ_3 (eddy diffusion parameter related to the trans-column velocity biases controlled by a flow mechanism). Note that we deliberately selected a weekly retained compound for which even small trans-column velocity biases would largely impact its HETP. On the other hand, the extra-column volume contributions could be accurately measured and the full peak integration method was chosen in order to measure the corrected HETPs. Finally, we conclude on the effect of the column inner diameter on the radial homogeneity of packed bed made of sub-3 μm core–shell particles.

4.1. Heat friction with core–shell particles

It is known from simple experimental results that viscous friction begins to deteriorate the column efficiency when the heat power generated inside the column exceeds 5 W/m, with pure acetonitrile as the eluent and fully porous BEH-C_{18} particles [2], provided that the column is left under still-air conditions and that the retention factor of the sample is moderate ($k \simeq$ 1–2). Table 2 lists the largest heat power measured with the nine columns tested. It is noteworthy that this power is always less than 6 W/m for all narrow-bore columns. In contrast, it may be as large as 20 W/m with 4.6 mm I.D. columns packed with either 2.7 μm Halo, 2.7 μm Poroshell120, or 2.6 μm Kinetex shell particles. The highest power reached is about 30 W/m with the 4.6 × 100 mm column packed with 1.7 μm Kinetex particles. Because the heat liberated in the column is directly proportional to the flow rate squared, the maximum flow rate considered in the multi variate regression analysis regarding the 4.6 mm I.D. columns should be 1.6 mL/min (2.7 μm particles) and 1.30 mL/min (1.7 μm particles) because the term h_{Heat} was neglected in the general expression of the reduced HETP in Eq. (2).

Using an aqueous mixture of acetonitrile and water (instead of pure acetonitrile) and core–shell particles (instead of fully porous particles) has an important effect on the heat conductivity of the packed bed. Typically, the heat conductivity of packed beds made of shell particles and flushed with aqueous eluent are about three times larger than that of beds made of fully porous particles eluted with a pure organic phase. Consequently, the threshold of heat power due to viscous friction above which the column efficiency

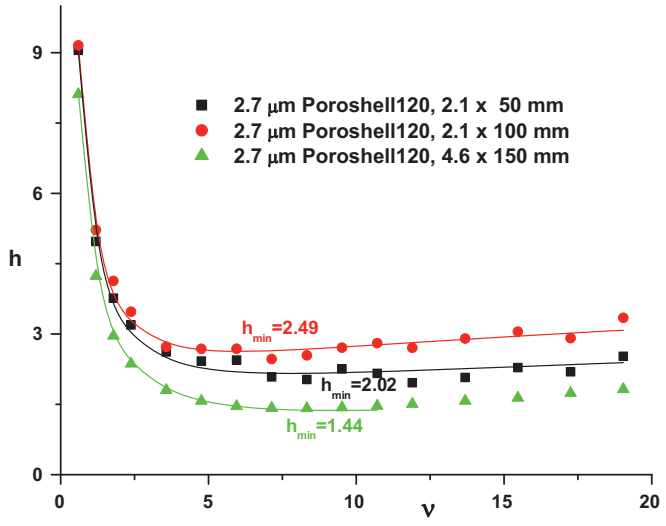

Fig. 1. Plots of the reduced plate heights of three analytical columns packed with the 2.7 μm Poroshell120 particles. The sample compound is naphthalene, the mobile phase is a mixture of acetonitrile and water (80/20, v/v), the temperature is set at T = 295 K. Note the smaller minimum reduced HETP with the large I.D. column (4.6 mm) relatively to the narrow-bore columns (2.1 mm I.D.). Comparison between the experimental reduced HETP (symbols) and the best theoretical HETP Eq. 1 (solid lines). The best optimized parameters Ω, ω_3, and λ_3 are listed in Table 2.

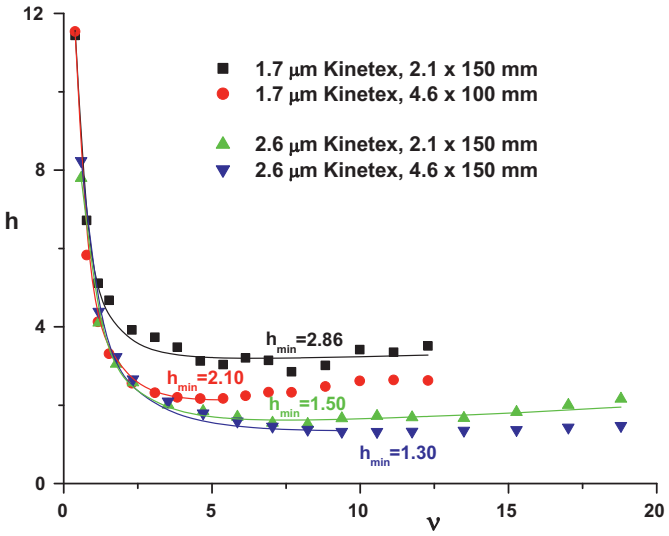

Fig. 2. Same plots as in Fig. 1 except the 1.7 μm Kinetex and 2.6 μm Kinetex particles. Again, note the decrease of the minimum reduced HETP when the column inner diameter increases from 2.1 to 4.6 mm.

begins to decrease sharply is larger [21,22]. In fact, Figs. 1–3 show nearly no parabolic deviation of the C-branch caused by frictional heating. This represents a clear advantage of shell over fully porous particles.

In conclusion, the best fit of the experimental data to the reduced HETP equation between 0.021 and 0.667 mL/min with narrow-bore columns and between 0.10 and 1.60 mL/min with 4.6 mm I.D. columns packed with shell particles does not require inclusion of the effects of frictional heating in Eq. (1).

4.2. Reduced experimental HETP plots

Figs. 1–3 compare the plots of the reduced plate heights of naphthalene on 4.6 mm I.D. and narrow-bore columns (2.1 mm I.D.) packed with 2.7 μm Poroshell120, 1.7 μm Kinetex, 2.6 μm Kinetex, and 2.7 μm Halo particles. With no exception, the minimum reduced HETP of the 4.6 mm I.D. columns is smaller than that of the narrow-bore columns packed with the same particles. The smallest HETP values measured with the 2.7 μm Halo 90 Å (h_{min}=1.56), 2.6 μm Kinetex 100 Å (h_{min} = 1.30), and 2.7 μm Poroshell 120 Å (h_{min} = 1.44) are in excellent agreement with similar results regarding the original performance of these columns [28,3,6,8]. Reducing the column inner diameter from 4.6 to 2.1 mm I.D. causes a significant loss in the optimum column efficiency, by of 16% (2.7 μm Halo), 27% (1.7 μm Kinetex), 13% (2.6 μm Kinetex), 29 % (2.7 μm Poroshell120 in a 2.1 × 50 mm column), and 42 % (2.7 μm Poroshell120 in a 2.1 × 100 mm column). The fact that comparable efficiency losses are observed for all brands of shell particles cannot be a coincidence. It reveals some specific kinetic pitfalls encountered either in the packing or in the use of narrow-bore columns, compared to the 4.6 mm I.D. columns. Recent reports [29–31] have shown that the minimum reduced HETP of narrow-bore columns packed with either 2.6 μm Kinetex or 2.7 μm Ascentis Express (Halo) were only around 2.0, results which confirm those observed in this work.

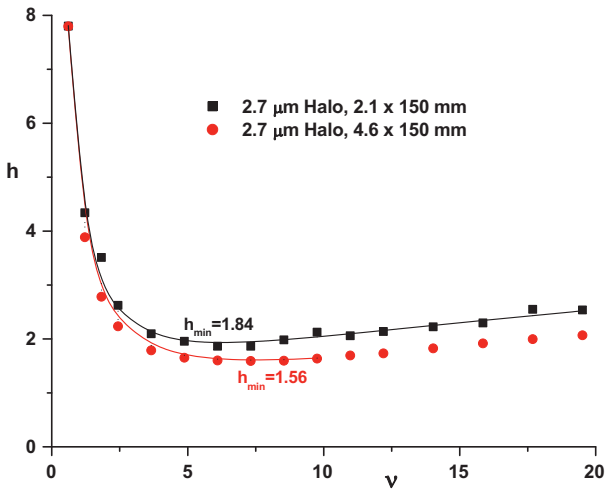

Fig. 3. Same plots as in Fig. 1 except the 2.7 μm Halo particles.

Interestingly, the C-branches of the 4.6 and 2.1 mm I.D. are nearly parallel to each other but slightly higher and steeper for the 2.1 than the 4.6 mm I.D. columns (see Figs. 1–3 and Table 2). Despite the expected contribution of the heat due to viscous friction to the reduced HETP of 4.6 mm I.D. columns at flow rates larger than 11.4 mL/min (see Section 4.1), the reduced HETPs of narrow-bore columns, which do not suffer from this cause of efficiency loss (P_f < 6 W/m), remains constantly larger than those of the 4.6 mm I.D. columns in the whole velocity range from ν = 7 to ν = 20. Clearly, this constant difference between the experimental HETP plots cannot be explained by a systematic larger longitudinal diffusion coefficient (B) of the narrow-bore columns. Although the particles packed in 4.6 and 2.1 mm I.D. columns originate from different batches, such a systematic difference would be unlikely. Furthermore, had this assumption been true, the difference between the reduced plate heights in the high velocity range would tend toward zero with increasing values of ν (since (B/ν) tends towards zero). The values of the coefficients $C_p + C_f$ vary between 0.019 and 0.030. The experimental slopes of the C branches measured between ν = 10 and ν = 20 are listed in Table 2. They vary from 0.036 to 0.123. Surprisingly, those of the narrow-bore columns are systematically larger than those observed for the 4.6 mm I.D. columns (see Table 2). This is due to the C branch being in part controlled by the eddy diffusion term, which increases with increasing linear velocity. For 10 <ν< 20, the fraction of the overall C coefficient accounted for by the trans-channel and short-range inter-channel velocity biases

are 0.004 and 0.005, respectively (Eq. (2)). Yet, adding up these contribution to the $C_p + C_f$ term does not allow a good match between the experimental and theoretical C coefficients. Therefore, both the differences between the C slopes and the h data in Figs. 1–3 should be explained by the same physical phenomenon, which must be the eddy diffusion related to velocity unevenness at a scale larger than short-range interchannel distances. Trans-column velocity biases are most certainly responsible for this difference. Neither frictional heating nor longitudinal diffusion and solid–liquid mass transfer can be responsible for the observations.

On another note, the comparison in Fig. 2 confirms that it is more difficult to pack efficiently 1.7 than 2.6 μm particles in either 2.1 or 4.6 mm I.D. column tubes. While the optimum reduced plate height is around 1.3–1.5 for 2.6 μm Kinetex particles, it exceeds 2.0 for 1.7 μm Kinetex particles. This result is not surprising but it is worth mentioning as a validation of the accuracy of our measurements.

In conclusion, we have identified the reason why narrow-bore columns are less efficient than 4.6 mm I.D. columns, they suffer from larger trans-column velocity biases. In the next Section, we discuss the fit of the HETP data to the theoretical HETP model presented in the theory section.

4.3. Why are narrow-bore columns less efficient than 4.6 mm I.D. columns?

The contribution of the trans-column velocity biases to the reduced HETP of naphthalene is written under the general form established by Giddings [12]:

$$h_{\text{trans-column}} = \frac{1}{(1/2\lambda_3) + (1/\omega_3 \nu)} \tag{17}$$

The parameter λ_3 in this equation is proportional to the square of the relative velocity biases between the central region of the column (where the velocity is uniform and the largest) and the wall region (where the velocity is the smallest), $\omega^*_{\beta,c}$ [12]. The term $2\lambda_3$ quantifies the expected eddy diffusion term when it is controlled by a sole flow mechanism. It is written [32,33]:

$$\lambda_3 = \frac{1}{2}\frac{p}{q}\frac{L}{d_p}\omega^{*2}_{\beta,c} \tag{18}$$

where L is the column length, and p and q are integer. The fraction (p/q) depends on the extent to which the local velocity is uniform in the central region of the column [33]. For instance, if we assume a parabolic flow profile across the column diameter $p = 1$ and $q = 12$. Therefore if $\omega^*_{\beta,c} \simeq 2\%$ [34,8], then λ_3 should physically be around 1.0 for 15 cm long columns packed with 2.6 μm particles. Besides, if we assume a polynomial of order twelve for the flow profile distribution, $(u(x) = u(0)[1 - \omega^*_{\beta,c}x^{12}])$, which describe a very flat profile in the center region of the column tube, then $p = 36$ and $q = 637$ [33]. Accordingly, λ_3 is expected to be equal to 0.7.

The parameter ω_3 describes eddy diffusion when it is governed by a sole diffusion process. It is proportional to the square of the relative velocity biases between the center and the wall region of the column and to the square of the normalized diffusion length, $\left(d_{tc}/d_p\right)^2$, across which the velocity biases take place. The largest possible value for d_{tc} is the column inner diameter, d_c. A large value for ω_3 suggests that the velocity bias extends over a large distance and *vice-versa*.

All the reduced HETP data were fitted to Eq. (1). To obtain the best fit, the values of three parameters were optimized, Ω, the ratio of the sample diffusivity in the porous shell to the bulk diffusion coefficient, λ_3, and ω_3. Ω was independently fixed in order to match exactly the values of the HETP measured at flow rates of 0.021 and 0.1 mL/min for the 2.1 and 4.6 mm I.D. columns, respectively. The impact of the parameters λ_3 and ω_3 on the HETP data measured for $\nu < 1$ is extremely weak. The average relative errors made on the determination of the best parameters ω_3 and λ_3 after the multi-linear regression analysis are equal to 13% and 22%. The objective function was the sum of the relative residual squared. All the results are given in Table 2. The excellent quality of the agreement between the experimental data and the best theoretical HETP curves is illustrated in Fig. 1 (Poroshell120), 2 (Kinetex), and 3 (Halo).

The best values of the parameter Ω were found between 0.70 and 1.20 for all the columns tested. These values are reasonable for a moderately retained compound in RPLC [35]. Under the experimental conditions used, naphthalene diffusivity through the porous shells is then comparable to the bulk diffusion coefficient, due to the large contribution of the surface diffusion of naphthalene in RPLC [36]. There is a slight variation from one brand of column to the next ($\Omega = 1.03$ with Halo 90 Å, 1.07 with Kinetex 100 Å, and 0.83 with Poroshell 120 Å) and even from one batch to the next for the same type of particles. The optimized parameters λ_3 were found to be between 0.80 and 1.60. This range of values for λ_3 is consistent with the expected values if the relative velocity bias across the column radius is of the order of 2%, the column length is 150 mm, and the particle size around 2.6 μm. Interestingly, all the results suggest that the λ_3 values are slightly smaller with 2.1 mm than with 4.6 mm I.D. column. This could mean that the relative velocity biases are barely smaller in narrow-bore than in large I.D. columns. Yet, the difference is not really significant given the robustness of the MLRA for this parameter (±22%).

The most interesting and unexpected finding is that the parameter ω_3 varies significantly from 4.6 mm I.D. to narrow-bore columns, given the precision on this parameter (±13%), since it increases from 0.06 to 0.13, 0.23 to 1.52, 0.03 to 0.08, and 0.03 to 0.35 for 2.7 μm Halo, 1.7 μm Kinetex, 2.6 μm Kinetex, and 2.7 Poroshell particles, respectively. From the previous analysis of the λ_3 coefficient, the velocity biases are comparable for the two column formats. Therefore, the difference in the ω_3 coefficients should be necessarily due to a difference in the normalized characteristic lengths, (d_{tc}/d_p), along which the sample has to radially diffuse. It is roughly 1.5 times larger with the 2.7 μm Halo particles, 2.5 times larger with the 1.7 μm Kinetex particles, 1.5 times larger with the 2.6 μm Kinetex particles, and 3 times larger with the 2.7 μm Poroshell particles.

It is possible to estimate the apparent characteristic diffusion distance, d_{tc}, if we assume that the relative velocity biases are equal to 2% for all the columns [34]. According to the construction of the term ω_3, this parameter is written [12]:

$$\omega_3 = \frac{d^2_{tc}\,\omega^{*2}_{\beta,c}}{2\,d^2_p} \tag{19}$$

This diffusion distance increases from 17 to 26 particle diameters with 2.7 μm Halo particles when the column diameter decreases from 4.6 to 2.1 mm. It increases from 34 to 87 and from 12 to 40 particle diameters with the 1.7 and 2.6 μm Kinetex particles, respectively. Finally, it increases from 13 to about 46 particle diameters for the 2.7 μm Poroshell120 particles. Note that this distance is maximum (150 μm) for the smallest 1.7 μm Kinetex particles in the narrow-bore column. This length accounts for about 14% of the column radius. The shortest radial diffusion distance is observed with the 2.6 μm Kinetex particles in 4.6 mm I.D. columns (32 μm) and represents no more than 1.5% of the column radius. As expected from previous and independent results obtained with retained compounds ($k \simeq 2$) and local electrochemical detection (benzoquinone sample), the trans-column eddy diffusion term in a 4.6 × 100 mm columns packed with 2.6 μm Kinetex particles is close to zero [33]. This conclusion is confirmed by the present experimental results obtained with 4.6 × 150 mm columns packed

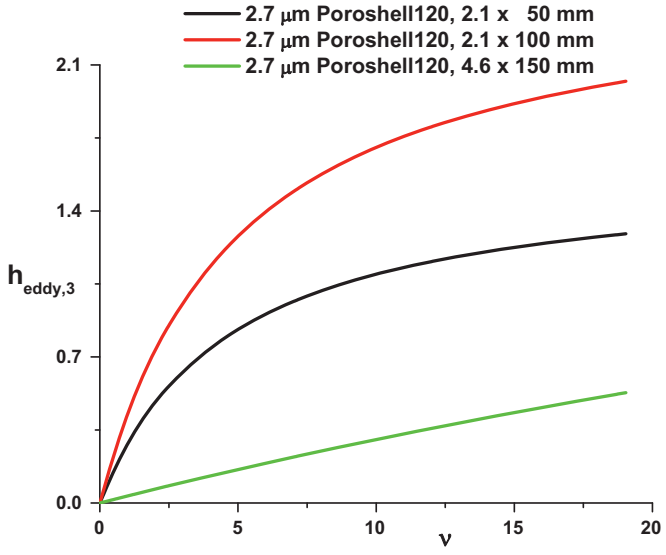

Fig. 4. Plots of the reduced long-range eddy diffusion term of naphthalene determined for the three columns packed with the 2.7 μm Poroshell120 shell particles. Note the large contribution of this eddy diffusion term with the narrow-bore columns.

with either 2.7 μm Poroshell, 2.7 μm Halo, or 2.6 μm Kinetex particles for which the parameter ω_3 is close to zero (<0.06).

In conclusion, the better kinetic performance of the 4.6 mm I.D. columns packed with fine sub-3 μm core–shell particles relatively to 2.1 mm I.D. columns is directly related to the shorter diffusion path over which the sample molecules have to diffuse in order to be exchanged between the eluent streamlines of extreme velocities.

4.4. Contribution of long-range velocity biases in narrow-bore and 4.6 mm I.D. columns

The previous two sections allowed us to demonstrate that: The difference in column efficiency between 4.6 and 2.1 mm I.D. columns packed with sub-3 μm core–shell particles is accounted for by a third eddy diffusion term with a characteristic length larger than the trans-channel ($\simeq(d_p/6)$) and the short-range interchannel ($\simeq d_p$) distances. The relative velocity biases are slightly smaller (or at least comparable) in narrow-bore columns than in 4.6 mm I.D. columns (see λ_3 coefficients in Table 2). The apparent characteristic length of this third eddy diffusion term is much shorter than the column inner radius for both column diameters (see ω_3 coefficients in Table 2) for moderately retained compounds, with $k \simeq 2$. This apparent characteristic length is larger in narrow-bore 2.1 mm (average 105 μm) than in 4.6 mm (average 42 μm) I.D. columns.

Accordingly, it would be better to call this third eddy diffusion term the long-range eddy diffusion term rather than the trans-column eddy diffusion term because the characteristic diffusion length is only a small fraction of the column inner diameter. These distances cover typically between a few dozens and 150 particle diameters. Figs. 4–6. compare plots of the long-range eddy diffusion term versus the reduced velocity for the different narrow-bore and 4.6 mm I.D. columns for 2.7 μm Halo, 1.7 μm Kinetex, 2.6 μm Kinetex, and 2.7 Poroshell particles, respectively. This eddy diffusion term is significantly larger than either the trans-channel or the short-range inter-channel eddy diffusion terms given in Eq. (2) and in reference [14]. For $\nu = 20$, the sum of these two eddy diffusion terms is no larger than 0.6 h unit. In fact, the reduced long-range eddy diffusion term is as large as 1.4, 2.2, 0.8, and 1.3 in 2.1 mm I.D. columns packed with 2.7 μm Poroshell, 1.7 μm Kinetex, 2.6 μm Kinetex, and 2.7 μm Halo particles, respectively. In the experimental range of reduced velocities accessible to small molecules, the

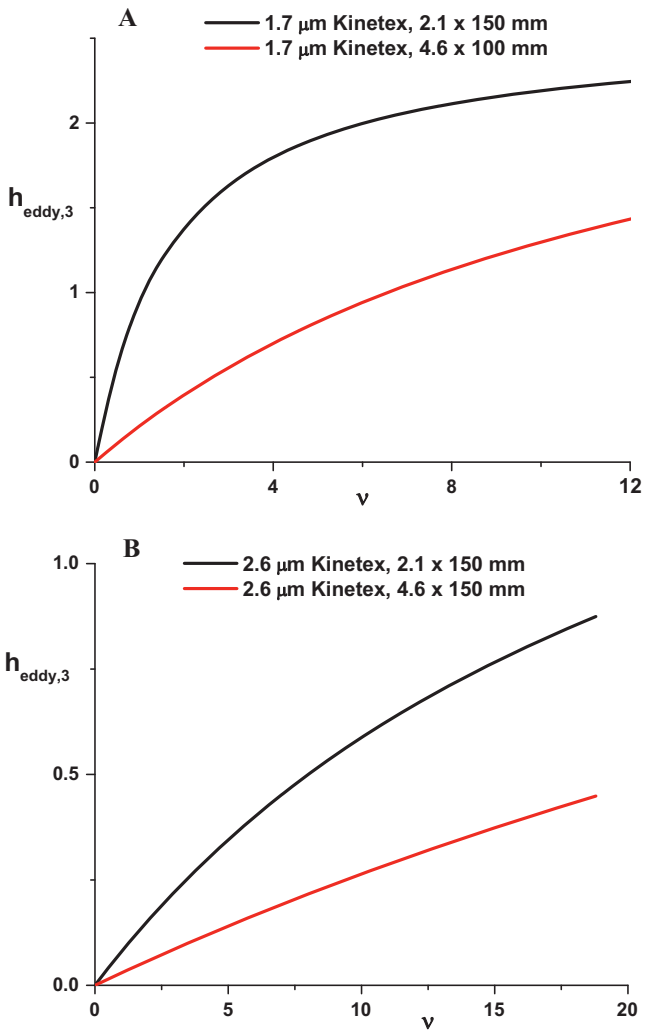

Fig. 5. Same plots as in Fig. 4 except with the 1.7 μm (A) and 2.6 μm (B) Kinetex particles. Note, again, the large contribution of this HETP term with the 2.1 mm I.D. column relatively to the 4.6 mm I.D. columns.

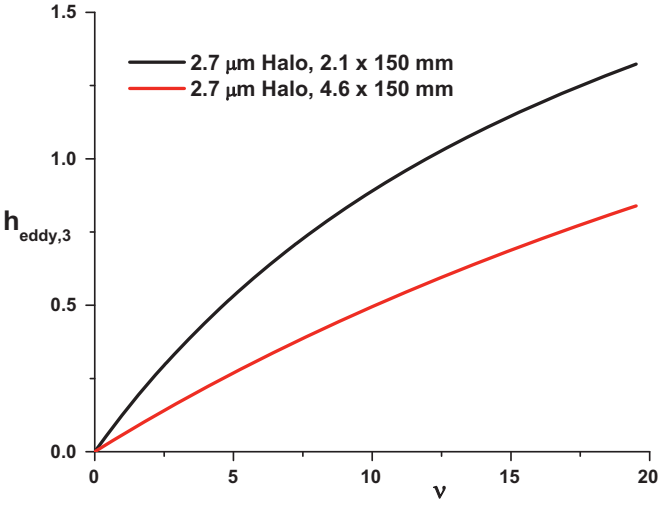

Fig. 6. Same plots as in Fig. 4 except with the 2.7 μm Halo particles.

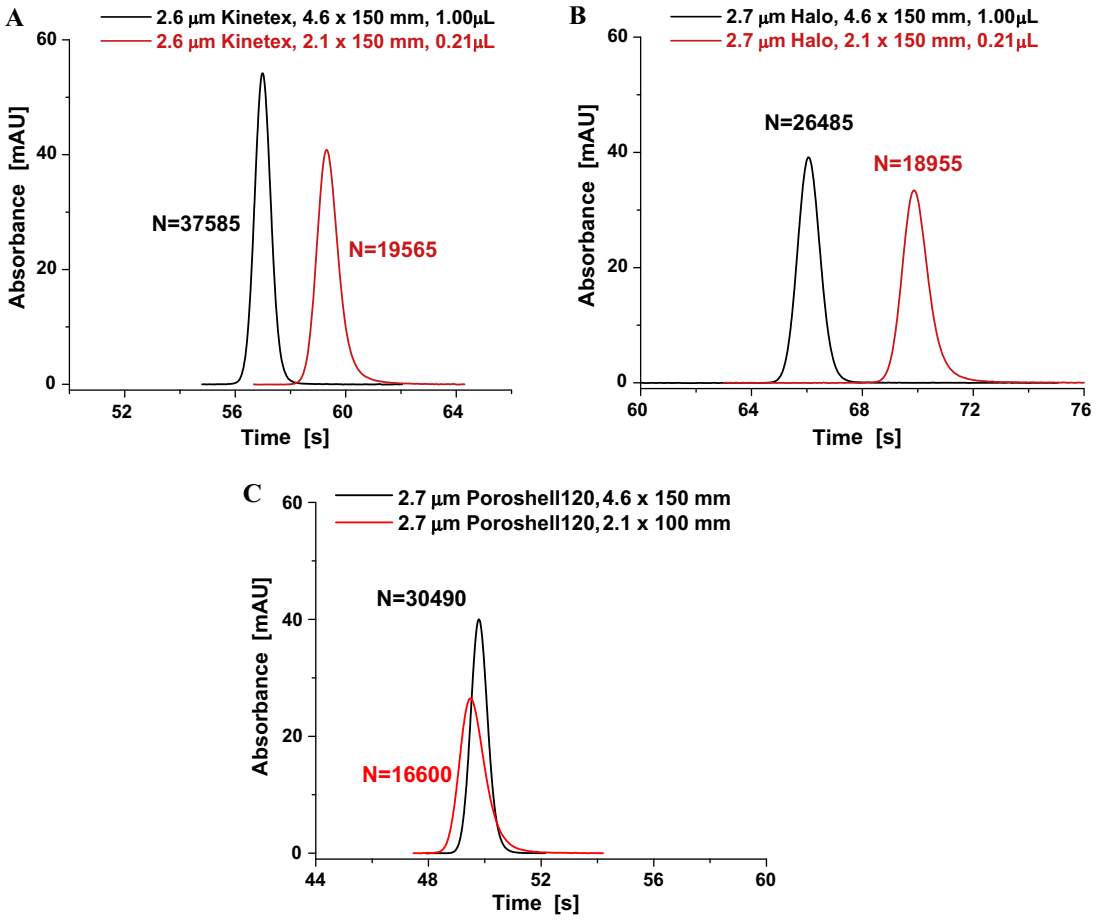

Fig. 7. Comparison between the experimental band profiles and column efficiencies measured with narrow-bore and 4.6 mm I.D. columns. Same experimental conditions as in Fig. 1 and the reduced interstitial linear velocity was set at $\nu = 19$. (A) 2.6 μm Kinetex shell particles. (B) 2.7 μm Halo shell particles. (C) 2.7 μm Poroshell120 particles. Note that the content of acetonitrile in the mobile phase was increased to (80/20, v/v) in order to generate comparable elution times on both columns (100 and 150 mm long). In all three cases, the enhanced peak tailing observed with the narrow-bore columns related to a long-range velocity bias from the wall to the center region of these 2.1 mm I.D. columns.

long-range inter-channel increases nearly linearly with increasing reduced velocity for the 4.6 mm I.D. columns and its slope ω_3 is extremely small. In contrast, with narrow-bore columns, the shape of this eddy diffusion term is strongly convex upward with a steeper initial slope, which is directly related to the larger characteristic diffusion distance.

4.5. Comparison of the band profiles in 2.1 and 4.6 mm I.D. columns

In this last section, we illustrate the difference between the kinetic performance of narrow-bore and 4.6 mm I.D. columns having the same length (150 mm Halo and Kinetex columns), at a the same reduced velocity close to 20. At such a velocity, frictional heating is significant in 4.6 mm I.D. columns but is negligible in narrow-bore columns. Yet, as shown in Fig. 7A (for 2.6 μm Kinetex) and 7B (for 2.7 μm Halo), the uncorrected efficiency of the large inner diameter columns remain larger (N=37585 and 26485 *versus* 19656 and 18955, respectively). Despite the larger volumes injected on the broader columns (1.00 *versus* 0.21 μL), the relative importance of the extra-column band broadening contribution (9.9 *versus* 4.9 μL^2, respectively) is larger with the narrow-bore than with the 4.6 mm I.D. columns. However, if we consider the Kinetex columns, the total variances ($((V_0^2(1+k)^2)/N$) are equal to 21.4 and 252 μL^2 with the 2.1 and 4.6 mm I.D. columns, respectively. The corrected efficiencies are then 25375 (initially 19656) and 39122 (initially 37585), respectively, still a significant difference. Therefore, as expected from Figs. 1 and 3 (where the corrected reduced plate heights are shown), the difference in column performance observed in Fig. 7A and B cannot be entirely attributed to the relative importance of the extra-column volume contributions. The larger long-range eddy diffusion term of the narrow-bore columns is consistent with the large extent of peak tailing observed with these columns whereas it is barely visible with 4.6 mm I.D. columns. Most likely, the migration linear velocity of the sample is slightly smaller in the region near the wall and reach a uniform value in the central region of the columns. This velocity gradient extends over an average distance of 100 μm for the 2.7 μm Halo, 1.7 and 2.6 μm Kinetex, and 2.7 μm Poroshell120 particles. This represents close to 10% of the column inner radius (1.05 mm). Fig. 7C illustrates well the link between a large long-range eddy diffusion term and the observed peak tailing with the 2.1 × 100 mm column packed with 2.7 μm Poroshell120 shell particles. In contrast, we must remember that the same average distance is about 40 μm with 4.6 mm I.D. columns, which represents only 1.7 % of the column inner radius (2.3 mm). This is consistent with the near absence of peak tailing for the 4.6 mm I.D. columns, as shown in Fig. 7A and B.

5. Conclusion

Our experimental results demonstrate that the kinetic performance of narrow-bore columns packed with any of the different brands of sub-3 μm core–shell particles are systematically inferior to that of those of 4.6 mm I.D. columns packed with the same mate-

rials. The reduced HETP of these columns were accurately measured using the exact first and second central moments, by numerical integration of the peak profiles. The analysis of the plots of these HETPs versus the reduced velocity in the range $0 < \nu < 20$ confirms that this difference in column performance is related to neither the longitudinal diffusion term, nor the solid–liquid mass transfer resistance term, nor to some frictional heating effect. In addition to the trans-channel and short-range inter-channel eddy diffusion terms, the fit of the experimental data to the general HETP equation implies the presence of a long-range eddy diffusion term which is solely responsible for the observed difference between the column performance.

Remarkably, the associated relative velocity biases are comparable or even slightly smaller within the 2.1 mm I.D. columns than within the 4.6 mm I.D. columns. This additional eddy diffusion term has a characteristic radial diffusion length which is much smaller than the inner column radius. Yet, it is as large as 10–15% of the internal radius of the narrow-bore columns but no longer than 2% of the inner radius of the 4.6 mm I.D. columns.

The results of this work strongly suggest that decreasing the column diameter enhances the effect of the column wall on the column efficiency. Most likely, still narrower columns (e.g. 500 μm or 1 mm i.d. columns) will exhibit even lower plate counts, possibly as long as the column to particle diameter ratio remains larger than about 7 [37]. Below that critical ratio, only wall effects take place and the bed becomes radially homogeneous again [38]. Current instruments are not suitable for the measurement of the intrinsic performance of such narrow columns, due to their large extra-column band broadening contributions.

The extrapolation of this work obviously addresses the problem of packing narrow-bore columns with very fine core–shell particles. This remains today both an art and a scientific discipline [17]. The challenge is demanding but the potential reward in terms of column efficiency could be important if radial bed homogeneity could be consistently achieved. Should we modify the nature of the inner surface of the column tubes? should we pack columns with particles still rougher than shell particles? should we narrow down the particle size distribution? Whatever significant gain could be made in column efficiency, new major changes in instrument technology will become necessary in order to achieve the full potential of these new columns.

Nomenclature

a	parameter defined in Eq. (9)
$A(\nu)$	reduced eddy diffusion term
B	reduced longitudinal diffusion coefficient
$C_f(\nu)$	external film mass transfer coefficient
C	total reduced solid–liquid reduced mass transfer coefficient
C_i	experimental sample concentration recorded at $t = t_i$ ($kg\,m^{-3}$)
C_p	trans-particle solid–liquid reduced mass transfer coefficient
d_c	inner diameter of the column stainless steel tube (m)
d_p	mean particle diameter (m)
d_c	column inner diameter (m)
d_{tc}	apparent radial diffusion distance across the column diameter (m)
D_m	bulk molecular diffusion coefficient (m^2/s)
F_v	flow rate (m^3/s)
h	total axial reduced column HETP
h_{heat}	reduced HETP due to frictional heating
k	retention factor
k_1	zone retention factor
K	equilibrium Henry's constant for the sample adsorption–desorption between the solid phase in the porous volume of the particle and the liquid eluent phase
L	column length (m)
P_f	heat power friction generated in the column per unit length (W/m)
ΔP	column pressure drop (Pa)
p	integer
q	integer
Sh	Sherwood number
t_i	experimental discretized time (s)
u	interstitial linear velocity (m/s)
$u_{(x)}$	interstitial linear velocity at the radial coordinate x (m/s)
$u_{(0)}$	interstitial linear velocity at the column center (m/s)
x	reduced radial coordinate in the column tube

Greek letters

ϵ_e	external column porosity
ϵ_p	particle porosity
ϵ_t	total column porosity
λ_3	limiting flow eddy diffusion coefficient for trans-column velocity biases
ω_3	diffusion eddy diffusion coefficient for trans-column velocity biases
μ_1	first moment of the concentration distribution in presence of the column (s)
$\mu_2^{'}$	second central moment of the concentration distribution in presence of the column (s^2)
$\mu_{1,ex}$	first moment of the concentration distribution in presence of the ZDV union connector (s)
$\mu_2^{'}$	second central moment of the concentration distribution in presence of the ZDV union connector (s^2)
ν	reduced interstitial linear velocity
Ω	ratio of the effective diffusivity of the sample in the porous shell to its bulk diffusion coefficient
$\omega^*_{\beta,c}$	relative velocity difference between the center region and the wall of the column
ρ	ratio of the solid non-porous core diameter to the core–shell particle diameter
$\sigma^2_{\nu,col.}$	column variance contribution (m^6)
$\sigma^2_{\nu,ex}$	instrument variance contribution (m^6)
$\sigma^2_{\nu,obs.}$	total variance observed (m^6)

Acknowledgements

This work was supported in part by the cooperative agreement between the University of Tennessee and the Oak Ridge National Laboratory. We thank Ron Majors (Agilent technologies, New Castle, DE, USA), Jack Kirkland and Joe DeStefano (Advanced material technologies, Wilmington, DE, USA), Tivadar Farkas and Carl Sanchez (Phenomenex, Torrance, CA, USA) for the generous gifts of the Poroshell120 and Kinetex columns used in this work and for fruitful discussions.

References

[1] U. Neue, N. Brady, S. Serpa, P. Iraneta, B. Alden, T. Walter, K. Wyndham, In 32nd International Symposium on High Performance Liquid Phase Separations and Related Techniques, Baltimore, MD, May 10–16, 2008.
[2] F. Gritti, G. Guiochon, J. Chromatogr. A 1217 (2010) 1485.
[3] J.J. DeStefano, T.J. Langlois, J.J. Kirkland, J. Chromatogr. Sci. 46 (2008) 254–260.
[4] S.A. Schuster, B.M. Wagner, B.E. Boyes, J.J. Kirkland, J. Chromatogr. Sci. 48 (2010) 566.
[5] F. Gritti, G. Guiochon, J. Chromatogr. A 1157 (2007) 289.
[6] F. Gritti, I. Leonardis, D. Shock, P. Stevenson, A. Shalliker, G. Guiochon, J. Chromatogr. A 1217 (2010) 1589.

[7] F. Gritti, G. Guiochon, J. Chromatogr. A 1217 (2010) 1604.
[8] F. Gritti, I. Leonardis, J. Abia, G. Guiochon, J. Chromatogr. A 1217 (2010) 3219.
[9] F. Gritti, G. Guiochon, J. Chromatogr. A 1217 (2010) 7677.
[10] F. Gritti, C. Sanchez, T. Farkas, G. Guiochon, J. Chromatogr. A 1217 (2010) 3000.
[11] F. Gritti, G. Guiochon, J. Chromatogr. A 1217 (2010) 5137.
[12] J. Giddings, Dynamics of Chromatography;, Marcel Dekker, New York, NY, 1965.
[13] A. Daneyko, S. Khirevich, U. Tallarek, In 35th International Symposium and Exhibit on High Performance Liquid Phase Separations and Related Techniques, HPLC2006, San Francisco, June 17–22, 2006.
[14] S. Khirevich, A. Daneyko, A. Holtzel, A. Seidel-Morgenstern, U. Tallarek, J. Chromatogr. A 1217 (2010) 4713.
[15] F. Gritti, G. Guiochon, Chem. Eng. Sci. 65 (2010) 6327.
[16] B.G. Yew, J. Ureta, R.A. Shalliker, E.C. Drumm, G. Guiochon, AIChE J. 49 (2003) 642.
[17] J.J. Kirkland, J.J. DeStefano, J. Chromatogr. A 1126 (2006) 50–57.
[18] R. Landauer, J. Appl. Phys. 23 (1952) 779–784.
[19] H. Davis, J. Am. Ceram. Soc. 60 (1977) 499–501.
[20] F. Gritti, G. Guiochon, AIChE. J. 2010, doi:10.1002/aic.12280.
[21] F. Gritti, G. Guiochon, J. Chromatogr. A 1217 (2010) 5069.
[22] F. Gritti, G. Guiochon, Chem. Eng. Sci. 65 (2010) 6310.
[23] K. Kaczmarski, G. Guiochon, Anal. Chem. 79 (2007) 4648.
[24] H. Lin, C. Horváth, Chem. Eng. Sci. 36 (1981) 47.
[25] K.J. Fountain, U.D. Neue, E.S. Grumbach, D.M. Diehl, G. Guiochon, J. Chromatogr. A 1216 (2010) 5979.
[26] C. Wilke, P. Chang, AIChE J. 1 (1955) 264.
[27] F. Gritti, G. Guiochon, J. Chromatogr. A, this issue.
[28] F. Gritti, M. Martin, G. Guiochon, Anal. Chem. 81 (2009) 3365.
[29] E. Olah, S. Fekete, J. Fekete, K. Ganzler, J. Chromatogr. A 1217 (2010) 3642.
[30] Y. Zhang, X. Wang, P. Mukherjee, P. Petersson, J. Chromatogr. A 1216 (2010) 4597.
[31] D.V. McCalley, J. Chromatogr. A 1217 (2010) 4561.
[32] F. Gritti, G. Guiochon, AIChE. J. 56 (2010) 1495.
[33] F. Gritti, G. Guiochon, J. Chromatogr. A 1217 (2010) 6350.
[34] J. Abia, K. Mriziq, G. Guiochon, J. Chromatogr. A 1216 (2009) 3185–3191.
[35] F. Gritti, G. Guiochon, Anal. Chem. 78 (2006) 5329.
[36] K. Miyabe, G. Guiochon, J. Chromatogr. A 1217 (2010) 3053.
[37] J. Knox, J. Parcher, Anal. Chem. 41 (1969) 1599.
[38] S. Hsieh, J. Jorgenson, Anal. Chem. 68 (1996) 1212.